

# Indenting fractal-edged elastic materials

D. F. S. Costa, J. H. M. Pontes, W. P. Ferreira, J. S. de Sousa, and C. L. N. Oliveira\*  
*Departamento de Física, Universidade Federal do Ceará, 60451-970 Fortaleza, Ceará, Brazil*

Surface roughness plays a crucial role in the accuracy of indentation experiments used to measure the elastic properties of materials. In this study, we present a computational analysis of how surface roughness, represented explicitly by fractal geometry, influences the mechanical properties of soft materials. We model two-dimensional elastic samples with a Koch fractal bottom surface, grown upward or downward to the fourth generation, referred to as fractal *down* and fractal *up*, respectively. The elastodynamics equations are solved numerically while a rigid punch indents the elastic sample from the top surface. By applying the Hertz model for mechanical contact, we determine the Young's modulus of the materials. Our findings reveal that fractal surfaces, especially those with dimensions comparable to the sample size, can significantly alter experimental measurement outcomes. In particular, the roughness of the substrate profoundly affects the measured elastic properties, as seen in scenarios involving cell elasticity. For instance, in the *down* fractal scenario, reductions in the measured elastic modulus range from 2% to 4%, while increases reach up to 40% in the *up* fractal scenario. These results underscore the importance of incorporating fractal geometry into the design and analysis of indentation experiments. This approach could significantly enhance our understanding and application of material characterization and mechanical testing, leading to more accurate and reliable results.

## I. INTRODUCTION

Interfacial effects profoundly influence the behavior of virtually every physical system [1], ranging from quantum devices [2, 3] and chemical compositions [4] to transport phenomena [5–7]. These effects can mislead estimations if not carefully considered, which is especially critical in experiments involving surface interactions. One common type of such experiment is indentation testing, where a hard tip is pressed into a material's surface to measure penetration depth and applied force, thereby evaluating mechanical properties. Traditional models like the Hertz mechanical contact model assume perfectly smooth surfaces and uniform stress distribution throughout the material. However, real-world materials often deviate from this ideal due to surface irregularities, such as microscale and nanoscale roughness in metals and polymers, respectively [8]. These discrepancies highlight the need for a nuanced approach to interpreting experimental data, considering the complex realities of material surfaces.

Surface roughness disrupts the assumption of uniform stress distribution, creating complex stress patterns that vary with the material's topographical features at different scales [9–11]. These irregularities can significantly alter experimental outcomes by inducing stress concentrations not fully accounted for by standard models [12, 13]. Addressing these complexities requires advanced modeling techniques and multi-scale mechanical characterization to assess a material's properties [14] accurately. Moreover, surface irregularities can compromise a material's yield strength, lead to premature plastic deformation, and interfere with measurements of elastic recovery, potentially resulting in incorrect assessments of a material's ability to revert to its original shape post-indentation [15].

Furthermore, nanoindentation assays on living cells provide insights into rheologic behaviors sensitive to their microenvironment and internal physical properties [16–20]. The interaction of proteins like integrins, which form focal adhesions connecting the cell to the substrate and activate intracellular signaling pathways, illustrates this sensitivity [21]. Cells can deform the contact surface on soft substrates such as the extracellular matrix, creating mechanical feedback that influences cell adhesion further. Such irregular adhesion topographies pose challenges and offer opportunities to explore cellular adaptation and mechanobiology [22]. Additionally, physiological processes or external stimuli driving changes in the cytoskeleton can significantly alter cell's mechanical properties [23, 24], evident in diseases like cancer where such properties serve as diagnostic markers [25–28]. Thus, understanding the influence of substrate roughness on these measurements is crucial for developing more effective diagnostic tools and enhancing our understanding of cellular mechanics in health and disease.

This study focuses on the impact of surface roughness, particularly fractal-like roughness characterized by self-similar patterns across scales, on the measurement of elastic properties. The presence of fractal geometry in surface roughness introduces substantial challenges, necessitating sophisticated models and analytical techniques for accurate

---

\*Electronic address: lucas@fisica.ufc.br

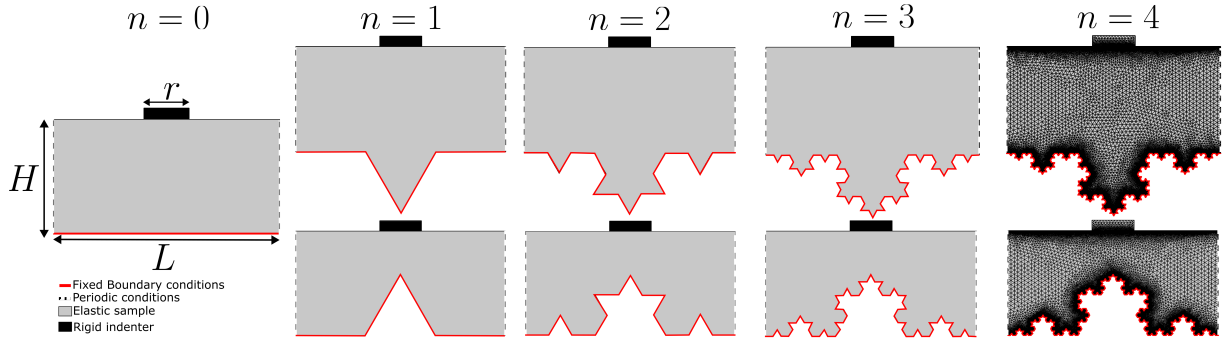


FIG. 1: Illustration of the indentation physical model, featuring an elastic sample colored in gray, with height  $H$  and length  $L$ , compressed from above by a rigid indenter of length  $r = L/5$ . The top surface, shown in a black solid line, is free to displace, while the bottom surface, represented by a red solid line, remains fixed. Periodic boundary conditions are applied on the sides to simulate an infinite medium. The bottom surface transforms according to the rules of a Koch fractal. At the first generation ( $n = 0$ ), the sample maintains a rectangular shape without fractal growth. Subsequent frames visually demonstrate the progressive growth of the fractal pattern from  $n = 1$  to  $n = 4$ , expanding either upwards or downwards. The numerical mesh for solving the elastodynamics equations is depicted for the ( $n = 4$ ) cases in up and down configurations.

property evaluation. We utilize numerical simulations to explore stress and strain distributions during indentation on surfaces modeled as Koch fractals, helping us understand how these patterns affect material behavior under stress and enabling us to design experiments that more accurately reflect the mechanical properties of materials with complex surfaces [29–31]. Such insights are critical in practical applications, especially in nanoindentation tests on soft materials with rough substrates, where surface roughness can directly affect the measurement of crucial parameters like elasticity [32, 33]. Understanding the fundamental mechanics governing complex material behavior under indentation is essential for advancing material design and selection in engineering applications and developing more effective diagnostic approaches in medical research [34–37].

## II. COMPUTATIONAL MODEL

Our model comprises a two-dimensional elastic medium characterized by Young’s modulus,  $E_s$ , a mass density,  $\rho$ , and a Poisson ratio,  $\nu$ . The top surface of this medium is free to move, while the lateral edges adhere to periodic boundary conditions to mitigate finite-size effects. Conversely, the bottom surface is fixed, evolving according to the  $n^{\text{th}}$  generation of a Koch fractal. This fixed boundary condition simulates a non-deformable substrate. The sample is compressed from above by a rigid rectangular indenter of length  $r$ , centrally positioned on the top surface, with an indentation given by  $\delta$ . As depicted in Fig. 1, at  $n = 0$ , the sample maintains a rectangular shape with height  $H$  and length  $L$ . However, the fractal may grow either downwards (in the same direction as the applied stress) or upwards (in the opposite direction), altering the sample’s mass by adding or removing material, respectively. Down-grown and up-grown fractals for  $n$  up to 4 are displayed, and we examine both scenarios. Only the bottom surface exhibits roughness, while the top remains flat to avoid numerical issues at the contact interface. Our simulations utilize parameters typical of Polyacrylamide gels, with  $E_s = 10^3$  Pa,  $\rho = 10^3$  kg/m<sup>3</sup>,  $\nu = 0.49$ , representing materials with elastic moduli ranging from hundreds to thousands of Pascal, by changing percentages of acrylamide and bis-acrylamide in PBS (phosphate-buffered saline) solution [38, 39].

The elastodynamics equations can effectively describe the deformation of a continuum elastic medium, which provides a comprehensive framework for understanding momentum conservation and the relationship between strain and stress [40, 41]. These equations are formulated as

$$\begin{aligned}\nabla \cdot \boldsymbol{\sigma} + \mathbf{f} &= \rho \ddot{\mathbf{u}}, \\ \boldsymbol{\varepsilon} &= \frac{1}{2} [(\nabla \mathbf{u})^T + \nabla \mathbf{u} + (\nabla \mathbf{u})^T \nabla \mathbf{u}],\end{aligned}$$

where  $\boldsymbol{\sigma}$  represents the Cauchy stress tensor,  $\boldsymbol{\varepsilon}$  the strain tensor,  $\mathbf{u}$  the displacement vector, and  $\mathbf{f}$  the volumetric forces. The stress and strain tensors are interconnected through the material’s constitutive relation, which, for small deformations, can be simplified by the generalized Hooke’s law  $\boldsymbol{\sigma} = \mathbf{C} : \boldsymbol{\varepsilon}$ , where the symbol  $:$  denotes the tensorial

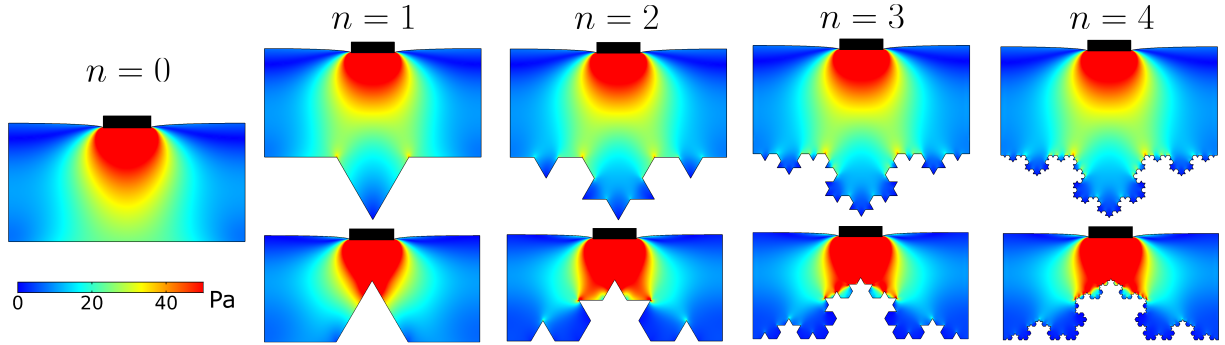


FIG. 2: The stress field for up to the fourth generation in both *up* and *down* fractal cases for  $H = 0.5$  cm and  $L = 1.0$  cm. The color gradient represents the Cauchy stress magnitude, measured in Pascals (Pa).

inner product, and the fourth-order stiffness tensor is given by

$$\mathbf{C} = \begin{bmatrix} \lambda + 2\mu & \lambda & \lambda & 0 & 0 & 0 \\ \lambda & \lambda + 2\mu & \lambda & 0 & 0 & 0 \\ \lambda & \lambda & \lambda + 2\mu & 0 & 0 & 0 \\ 0 & 0 & 0 & \mu & 0 & 0 \\ 0 & 0 & 0 & 0 & \mu & 0 \\ 0 & 0 & 0 & 0 & 0 & \mu \end{bmatrix}, \quad (1)$$

where  $\lambda = \nu E / [(1 + \nu)(1 - 2\nu)]$  and  $\mu = E / [2(1 + \nu)]$  are, respectively, the Lamé's first and second parameters.

In our analyses, we apply indentation up to 4% of  $H$ , leading to stationary conditions where  $\dot{\mathbf{u}} = 0$  and  $(\nabla \mathbf{u})^T \nabla \mathbf{u} = 0$ , with no external volumetric forces,  $\mathbf{f} = 0$ . The bottom surface is immovable due to fixed boundary conditions ( $\mathbf{u} = 0$ ). These conditions simplify the equations to

$$\nabla \cdot \boldsymbol{\sigma} = 0, \quad (2)$$

$$\boldsymbol{\varepsilon} = \frac{1}{2} [(\nabla \mathbf{u})^T + \nabla \mathbf{u}], \quad (3)$$

commonly known as the compatibility equations. These equations are solved using the commercial software *COMSOL Multiphysics*, which employs the finite element method to manage the computational complexities [42]. The results, including stress and strain distributions and the contact force,  $F_c$ , between the sample and the indenter for a given indentation  $\delta$ , are calculated and visually represented. The numerical mesh used for these calculations is shown in Fig. 1 for  $n = 4$ .

### III. RESULTS

The geometry of our 2-D model is straightforward, comprising a rectangular sample in contact with a similarly shaped rectangular indenter. One of the most fascinating aspects of our model is the incorporation of a rough surface in the form of a fractal generation at its base. This distinctive feature is a critical element of our study. It allows us to explore the effects of self-similarity across multiple scales, and more importantly, it alters the stress distribution within the material. Fig. 2 provides a detailed view of the stress field distribution within the sample across various fractal generations for both *up* and *down* geometries. As expected, for a surface without fractal growth ( $n = 0$ ), the stress field disperses uniformly from the indenter's contact region throughout the sample. However, as  $n$  increases, the stress field becomes concentrated at pointed regions on the fractal surface, disrupting the uniform distribution. This effect is further accentuated in the upward fractal orientation, where high-stress concentrations are observed on the bottom surface, as indicated by the red regions in the figure. Although measuring stress maps in bulk samples is challenging, experimental techniques can be applied to obtain such information on surfaces [43], allowing for a potential comparison with our results.

The Hertz model for mechanical contact provides critical insights into the indentation of purely elastic materials. Using a rigid flat-ended cylindrical indenter results in a linear increase in contact force with indentation depth  $\delta$  [44, 45], as expressed by

$$F_c(\delta) = \frac{2r}{(1 - \nu^2)} E \delta, \quad (4)$$

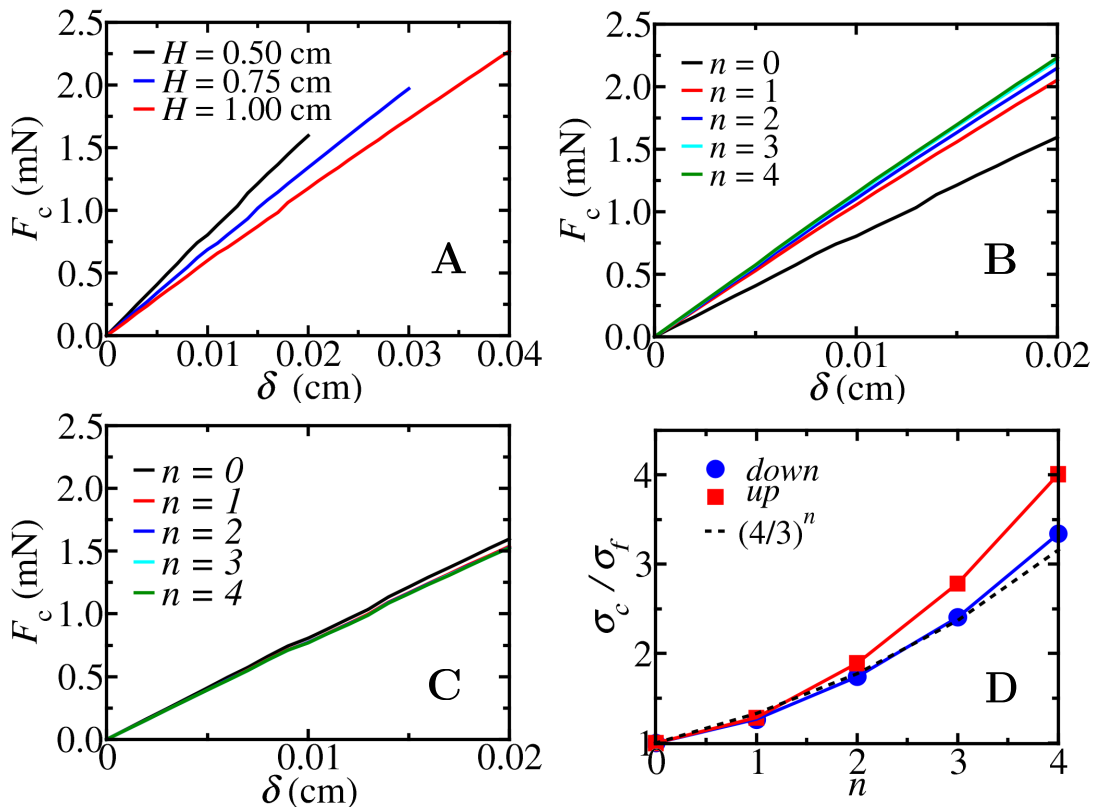


FIG. 3: (A) Contact force curve versus indentation for different values of  $H$  in the flat sample ( $n = 0$ ). The slope of these curves reflects the sample's rigidity. Frames (B) and (C) show similar curves to (A) but for a fixed  $H = 0.5$  cm and several fractal generations ( $n$ ) in the *up* and *down* fractal scenarios, respectively. These plots effectively demonstrate the influence of fractal geometry on the force-indentation relationship, with significant differences observed in comparison to the flat sample. Additionally, frame (D) depicts the ratio of the stress exerted on the contact surface,  $\sigma_c$ , to that on the fractal surface,  $\sigma_f$ , as the fractal generation increases. This graph shows us the accumulation of the stress through the elastic sample. Both *down* and *up* fractal cases slightly diverge from the growth behavior of the Koch fractal,  $(4/3)^n$ , as  $n$  increases.

where  $E$  represents the effective Young's modulus. This relationship directly reflects Hooke's Law, where the stiffness constant,  $k = \frac{2r}{(1-\nu^2)}E$ , can be calculated from the slope of the contact force curve. We show that  $E$  depends on  $n$ , indicating a divergence from the actual Young's modulus of the sample,  $E_s$ .

Figure 3(A) displays the Hertz curve for the flat case ( $n = 0$ ), showing that the spring constant decreases with increasing sample height, consistent with finite-size effects [46]. The influence of fractal geometry on these measurements is evident in the force curves in Figs. 3(B) and (C). Fractal generation slightly reduces stiffness, with a more significant impact in the upward scenario. By analyzing the slope of these curves, we can infer changes in stiffness, illustrating how fractal geometry influences the material's response to indentation. These results suggest that as fractal generation  $n$  increases, the stiffness modulus  $E$  tends towards a specific value significantly influenced by the sample height.

To calculate the ratio between the average stress on the contact surface,  $\sigma_c$ , and that on the fractal surfaces,  $\sigma_f$ , we assume the stress is uniformly transmitted along the vertical direction through the sample. In this scenario, the disparity between the stresses should compensate for the difference in the perimeter of each surface. Thus,  $\sigma_f \propto 1/P(n)$ , where  $P(n) = (4/3)^n L$  is the perimeter of the  $n^{\text{th}}$  generation of the Koch fractal initial length  $L$  [47]. Similarly,  $\sigma_c \propto 1/S(\delta)$ , where  $S(\delta)$  is the actual length on the top surface, which depends on the indentation due to its deformability. For small indentations,  $S(\delta) \approx L$ . Therefore, the ratio between the stresses can be computed as

$$\frac{\sigma_c}{\sigma_f} \propto \frac{P(n)}{S(\delta)} \propto \left(\frac{4}{3}\right)^n \frac{L}{S(\delta)} \approx \left(\frac{4}{3}\right)^n, \quad (5)$$

yielding the same growth rule as the Koch fractal. However, since the stress is not uniformly distributed along the sample, the ratio  $\sigma_c/\sigma_f$  as a function of the fractal generation  $n$ , shown in Fig. 3(D), slightly diverges from this prediction. The divergence observed in the simulations, both in the *up* and *down* fractal cases, from the  $(4/3)^n$

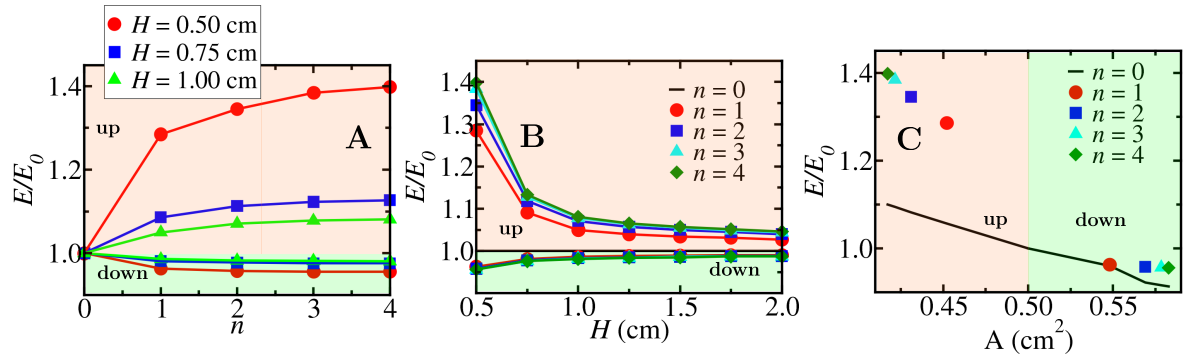


FIG. 4: Young's modulus,  $E(H, n)$ , measured in a sample with height  $H$  and generation  $n$ , normalized to the value of  $E$  with the same  $H$  but  $n = 0$ , which we call  $E_0$ , in both *down* and *up* fractal orientations. (A) shows how  $E/E_0$  changes with  $n$  for different values of  $H$  while (B) shows changing with  $H$  for different values of  $n$ . In frame (C), we adjust  $H$  to compensate for the area lost or gained due to fractal growth, keeping the sample's area constant and equal to  $HL$ , the area without fractal boundary.

behavior highlights the non-uniformity of the stress propagation due to the emergence of stress concentration areas with increasing  $n$ .

The graphs in Fig. 4 present the effective Young's modulus normalized by the value,  $E_0$  where no fractal is grown with height  $H$ , for both *down* and *up* cases. By normalizing Young's modulus, we can track the percentage changes as fractal generation progresses compared to a smooth sample. Fig. 4(A) demonstrates that fractal surfaces can decrease or increase the measured elastic modulus. In the *down* fractal scenario, reductions are generally below 5%, while in the *up* fractal scenario, increases can reach 40%. As expected,  $E/E_0$  approaches one as  $H$  increases, as shown in frame (B). As  $H$  increases, the influence of surface roughness diminishes, with both *up* and *down* fractals converging to typical values, illustrating the lesser impact of fractal features on larger samples. Increasing  $H$  leads to a slow convergence of the analytical Young's modulus to the value input in the numerical model. In Fig. 4(C), the fractal was generated at a specific  $n$  while  $H$  was adjusted to conserve the same area of  $n = 0$  (equal to  $HL$ ). The solid black line represents the expected behavior for flat samples. Even with the area adjustment, the *up* fractal configuration maintains a relatively high Young's modulus. These graphs effectively demonstrate the substantial impact of fractal generation and configuration on the elastic properties, underscoring how fractal dimensions influence material behavior under mechanical stress. We also analyze different cases with varying  $L$  ( $L = 2H, 6H, 10H$ ) for both *up* and *down* scenarios, as depicted in Fig. 5(A-C) for  $L = 10H$  and  $n = 4$ . Normalization shows that the effects of fractal generation remain constant despite the increase in  $L$ , as demonstrated in Fig. 5(D).

#### IV. CONCLUSIONS

Our work reveals the significant impact of surface roughness, particularly fractal geometry, on the accuracy of indentation experiments used to measure the elastic properties of materials. We have demonstrated that the fractal nature of the bottom surface is a critical factor in scenarios involving thin films or textured substrates, where it significantly alters the mechanical response during indentation. The structural complexity introduced by fractal patterns has essential implications for stress distribution and the force-indentation relationship. Specifically, in the *down* fractal scenario, where the material is added, reductions in the elastic modulus ranged between 2% and 4% compared to the case without a fractal boundary, depending on the sample height  $H$ . Conversely, in the *up* fractal scenario, where the material is removed, increases in the modulus reached up to 40%. We also analyzed cases where the amount of material was conserved by adjusting the height  $H$  to maintain the same area as a smooth sample. Even in these scenarios, the fractal boundary significantly influenced the elastic measurements, demonstrating that fractal geometry can lead to deviations from expected mechanical behavior, regardless of material conservation. Our findings not only highlight the necessity of accounting for surface roughness, particularly fractal geometry, in the design and analysis of indentation experiments, but also point to potential applications in biophysics. Particularly, our work could contribute to a better understanding of rheological measurements in living cells. The influence of fractal-like surface roughness could help explain the variations observed in the mechanical properties of cells, especially in the context of cellular adhesion and interactions with substrates of varying stiffness and roughness. This potential for practical applications should inspire and encourage further exploration in this field. While our research is focused on deterministic fractals, it opens up substantial potential for future studies to explore random fractals, such as self-affine

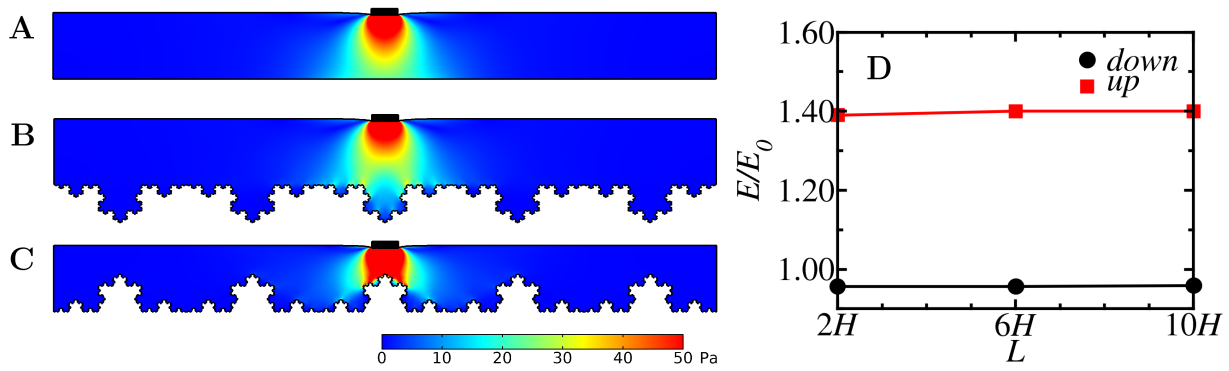


FIG. 5: The magnitude of the Cauchy stress, measured in Pascals (Pa), is represented by a color gradient for  $H = 0.5$  cm and  $L = 10H$ . The sample without fractal ( $n = 0$ ) is shown in (A), while the fractal cases *up* in (B) and *down* (C) for  $n = 4$ . The ratio  $E/E_0$ , defined in Fig. 4, is maintained regardless of the length  $L$ .

surfaces or other geometric roughness models. These investigations could lead to the development of more effective diagnostic tools and material design strategies in engineering and medical research.

#### Acknowledgments

The authors acknowledge the financial support from the Brazilian agencies CNPq, CAPES, and FUNCAP.

Author Declarations: The authors have no conflicts to disclose

- 
- [1] D. Allara, A perspective on surfaces and interfaces, *Nature* 437 (2005) 638. <https://doi.org/10.1038/nature04234>
  - [2] C. L. N. Oliveira, J. A. K. Freire, V. N. Freire, and G. A. Farias, Effects of interfacial profiles on quantum levels in  $\text{In}_x\text{Ga}_{1-x}\text{As}/\text{GaAs}$  graded spherical quantum dots, *App. Surf. Sci.* 237 (2004) 266. <https://doi.org/10.1016/j.apsusc.2004.06.048>
  - [3] C. L. N. Oliveira, J. A. K. Freire, V. N. Freire, and G. A. Farias, Inhomogeneous broadening arising from interface fluctuations in strained  $\text{In}_x\text{Ga}_{1-x}\text{As}/\text{GaAs}$  and  $(\text{In}_u\text{Ga}_{1-u}\text{As})_v(\text{InP})_{1-v}/\text{InP}$  quantum wells, *App. Surf. Sci.* 234 (2004) 38. <https://doi.org/10.1016/j.apsusc.2004.05.055>
  - [4] M. Prutton, *Introduction to Surface Physics*, Oxford University Press, 1994.
  - [5] J. S. Andrade Jr., E. A. A. Henrique, M. P. Almeida, M. H. A. S. Costa, Heat transport through rough channels, *Phys. A* 339 (2004) 296. <https://doi.org/10.1016/j.physa.2004.03.066>
  - [6] C. L. N. Oliveira, F. K. Wittel, J. S. Andrade Jr, H. J. Herrmann, Invasion percolation with a hardening interface under gravity, *Int. J. Mod. Phys. C* 21 (2010) 903. <https://doi.org/10.1142/S0129183110015555>
  - [7] E. K. Lenzi, A. A. Tateishi, H. V. Ribeiro, M. K. Lenzi, G. Gonçalves and L. R. da Silva, Fractional diffusion equation, boundary conditions and surface effects, *J. Stat. Mech.* (2014) P08019. <https://doi.org/10.1088/1742-5468/2014/08/P08019>
  - [8] H. G. Chuah, W. H. Tan, B. P. Chang, T. S. Khoo, C. Y. Khor, and H. G. How, The influence of surface roughness on material dislocation of microindentation using bonded interface technique, *Tribology - Materials, Surfaces & Interfaces* 13 (4) (2019) 191. <https://doi.org/10.1080/17515831.2019.1643074>
  - [9] H. B. Yang and M. Dai, Influence of surface roughness on the stress field around a nanosized hole with surface elasticity, *Z. Angew. Math. Phys* 69 (2018) 127. <https://doi.org/10.1007/s00033-018-1022-x>
  - [10] P. Mohammadi and P. Sharma, Atomistic elucidation of the effect of surface roughness on curvature-dependent surface energy, surface stress, and elasticity, *Appl. Phys. Lett.* 100 (2012) 133110. <https://doi.org/10.1063/1.3695069>
  - [11] A. McMillan, R. Jones, D. Peng and G. A. Chechkin, A computational study of the influence of surface roughness on material strength, *Meccanica* 53 (2018) 2411. <https://doi.org/10.1007/s11012-018-0830-6>
  - [12] Y. Xiao, L. Wu, J. Luo, and L. Zhou, Mechanical response of thin hard coatings under indentation considering rough surface and residual stress, *Diamond and Related Materials* 108 (2020) 107991. <https://doi.org/10.1016/j.diamond.2020.107991>
  - [13] A. Tiwari and B. N. J. Persson, Cylinder-flat contact mechanics with surface roughness, *Tribology Letters* 69 (1) (2021) 4. <https://doi.org/10.1007/s11249-020-01380-z>
  - [14] G. Peng, Y. Liu, F. Xu, H. Jiang, W. Jiang, and T. Zhang, On determination of elastic modulus and indentation hardness by instrumented spherical indentation: influence of surface roughness and correction method, *Mater. Res. Express* 10 (8) (2023) 086503. <https://doi.org/10.1088/2053-1591/acebbb>

- [15] A. Tiwari, A. Almqvist, and B. N. J. Persson, Plastic Deformation of Rough Metallic Surfaces, *Tribol. Lett.* 68 (2020) 129. <https://doi.org/10.1007/s11249-020-01368-9>
- [16] J. S. de Sousa, J. A. C. Santos, E. B. Barros, L. M. R. Alencar, W. T. Cruz, M. V. Ramos, and J. Mendes Filho, Analytical model of atomic-force-microscopy force curves in viscoelastic materials exhibiting power law relaxation, *J. Appl. Phys.* 121 (2017) 034901. <https://doi.org/10.1063/1.4974043>
- [17] J. S. de Sousa, R. S. Freire, F. D. Sousa, M. Radmacher, A. F. B. Silva, M. V. Ramos, A. C. O. Monteiro-Moreira, F. P. Mesquita, M. E. A. Moraes, R. C. Montenegro, and C. L. N. Oliveira, Double power-law viscoelastic relaxation of living cells encodes motility trends, *Sci. Rep.* 10 (2020) 4749. <https://doi.org/10.1038/s41598-020-61631-w>
- [18] I. V. M. Lima, A. V. S. Silva, F. D. Sousa, W. P. Ferreira, R. S. Freire, C. L. N. Oliveira, and J. S. de Sousa, Measuring the viscoelastic relaxation function of cells with a time-dependent interpretation of the Hertz-Sneddon indentation model, *Heliyon* 10 (2024). <https://doi.org/10.1016/j.heliyon.2024.e30623>
- [19] A. L. D. Moura, W. V. Santos, F. D. Sousa, R. S. Freire, C. L. N. Oliveira, and J. S. Sousa, Viscoelastic relaxation of fibroblasts over stiff polyacrylamide gels by atomic force microscopy, *Nano Ex.* 4 (3) (2023) 035008. <https://doi.org/10.1088/2632-959X/acf1b8>
- [20] D. E. Discher, P. Janmey, and Y.-L. Wang, Tissue cells feel and respond to the stiffness of their substrate, *Science* 310 (2005) 1139. <https://doi.org/10.1126/science.1116995>
- [21] H. Parameswaran, K. R. Lutchien, and B. Suki, A computational model of the response of adherent cells to stretch and changes in substrate stiffness, *J. Appl. Physiol.* 116 (2014) 825. doi:10.1152/jappphysiol.00962.2013
- [22] C. Rianna and M. Radmacher, Influence of microenvironment topography and stiffness on the mechanics and motility of normal and cancer renal cells, *Nanoscale* 9 (31) (2017) 11222. <https://doi.org/10.1039/C7NR02940C>
- [23] Q. Wen and P. A. Janmey, Polymer physics of the cytoskeleton, *Curr. Opin. Solid State and Materials, Science* 15 (2) (2011) 177. <https://doi.org/10.1016/j.cossms.2011.05.002>
- [24] X. Trepatt, G. Lenormanda and J. J. Fredberg, Universality in cell mechanics, *Soft Matter* 4 (9) (2008) 1750. <https://doi.org/10.1039/B804866E>
- [25] L. M. Rebelo, J. S. Sousa, J. Mendes Filho, and M. Radmacher, Comparison of the viscoelastic properties of cells from different kidney cancer phenotypes measured with atomic force microscopy, *Nanotechnol.* 24 (5) (2013) 055102. <https://doi.org/10.1088/0957-4484/24/5/055102>
- [26] M. Lekka, Discrimination between normal and cancerous cells using AFM, *BioNanoSci* 6 (2016) 65. <https://doi.org/10.1007/s12668-016-0191-3>
- [27] D. Fisseha and V. K. Katiyar, Analysis of Mechanical Behavior of Red Cell Membrane in Sickle Cell Disease, *Appl. Math.* 2 (2012) 40. <https://doi.org/10.5923/j.am.20120202.08>
- [28] Y. Abidine, A. Giannetti, J. Revilloud, V. M. Laurent, and C. Verdier, Viscoelastic properties in cancer: From cells to spheroids, *Cells* 10 (7) (2021) 1704. <https://doi.org/10.3390/cells10071704>
- [29] M. Bogahawaththa, D. Mohotti, P. J. Hazell, H. Wang, K. Wijesooriya, and C. K. Lee, Energy absorption and mechanical performance of 3D printed Menger fractal structures, *Engineering Structures* 305 (2024) 117774. <https://doi.org/10.1016/j.engstruct.2024.117774>
- [30] P. Pavón-Domínguez, G. Portillo-García, A. Rincón-Casado, and L. Rodríguez-Parada, Influence of the fractal geometry on the mechanical resistance of cantilever beams designed through topology optimization, *Appl. Sci.* 11 (22) (2021) 10554. <https://doi.org/10.3390/app112210554>
- [31] J. Wang, Y. Zhang, N. He, and C. H. Wang, Crashworthiness behavior of Koch fractal structures, *Materials & Design* 144 (2018) 229. <https://doi.org/10.1016/j.matdes.2018.02.035>
- [32] A. Roy and K. Vemaganti, Fractal surface-based three-dimensional modeling to study the role of morphology and physiology in human skin friction, *Surf. Topogr.: Metrol. Prop.* 12 (1) (2024) 015006. <https://doi.org/10.1088/2051-672X/ad1fda>
- [33] L. Afferrante, G. Violano, and G. Carbone, Exploring the dynamics of viscoelastic adhesion in rough line contacts, *Sci. Rep.* 13 (1) (2023) 15060. <https://doi.org/10.1038/s41598-023-39932-7>
- [34] I. Sokolov, Editorial - Fractals: a possible new path to diagnose and cure cancer? *Future Oncol.* 11 (22) (2015) 3049. <https://doi.org/10.2217/fon.15.211>
- [35] J. W. Baish and R. K. Jain, Fractals and Cancer, *Cancer Res.* 60 (2000) 3683.
- [36] R. Sedivy and R. M. Mader, Fractals, Chaos, and Cancer: Do They Coincide? *Cancer Investigation* 15 (6) (1997) 601. <https://doi.org/10.3109/07357909709047603>
- [37] M. E. Dokukin, N. V. Guz, R. M. Gaikwad, C. D. Woodworth, and I. Sokolov, Cell surface as a fractal: normal and cancerous cervical cells demonstrate different fractal behavior of surface adhesion maps at the nanoscale, *Phys. Rev. Lett.* 107 (2) (2011) 028101. <https://doi.org/10.1103/PhysRevLett.107.028101>
- [38] M. A. Caporizzo, C. M. Roco, M. C. C. Ferrer, M. E. Grady, E. Parrish, D. M. Eckmann, and R. J. Composto, Strain-rate Dependence of Elastic Modulus Reveals Silver Nanoparticle Induced Cytotoxicity, *Nanobiomed.* 2 (2015) 9. <https://doi.org/10.5772/61328>
- [39] J. R. Tse and A. J. Engler, Preparation of Hydrogel Substrates with Tunable Mechanical Properties, *Current Protocols in Cell Biology* 47 (2010) 10.16.1. <https://doi.org/10.1002/0471143030.cb1016s47>
- [40] A. J. M. Spencer, Continuum mechanics, Courier Corporation, 2004.
- [41] R. Zielinski et al., Finite element analysis of traction force microscopy: influence of cell mechanics, adhesion, and morphology, *J. Biomech. Eng.* 135 (7) (2013) 071009-1. <https://doi.org/10.1115/1.4024467>
- [42] COMSOL Multiphysics® [www.comsol.com](http://www.comsol.com). COMSOL AB, Stockholm, Sweden.
- [43] B. Suki, Y. Hu, N. Murata, J. Imsirovic, J. R. Mondoñedo, C. L. N. Oliveira, N. Schaible, P. G. Allen, R. Krishnan, E. Bartolák-Suki, A microfluidic chamber-based approach to map the shear moduli of vascular cells and other soft materials,

- Sci. Rep. 7 (2017) 2305. <https://doi.org/10.1038/s41598-017-02659-3>
- [44] I. Sneddon, The relation between load and penetration in the axisymmetric boussinesq problem for a punch of arbitrary profile, *Int. J. Eng. Sci.* 3 (1965) 47. [https://doi.org/10.1016/0020-7225\(65\)90019-4](https://doi.org/10.1016/0020-7225(65)90019-4)
- [45] F. B. de Sousa, P. K. V. Babu, M. Radmacher, C. L. N. Oliveira, J. S. de Sousa, Multiple power-law viscoelastic relaxation in time and frequency domains with atomic force microscopy, *J. Phys. D: Appl. Phys.* 54 (2021) 335401. <https://doi.org/10.1088/1361-6463/ac02fa>
- [46] D. F. S. Costa, J. L. B. de Araújo, C. L. N. Oliveira, J. S. de Sousa, Nanoindentation in finite thickness viscoelastic materials, *Journal of Applied Physics* 132 (2022) 214701. <https://doi.org/10.1063/5.0127403>
- [47] J. Feder, *Fractals*, 5th ed., Springer Science & Business Media, 2013.